Investigation on the fracture mechanism of homogenized micro-crack crushing technology for portland cement concrete pavement rehabilitation

Cite as: AIP Advances **9**, 075113 (2019); https://doi.org/10.1063/1.5111055
Submitted: 22 May 2019 . Accepted: 08 July 2019 . Published Online: 19 July 2019

Wenjie Li, Qunlei Zhang, Zihan Zhi, Chun Feng, Yingchun Cai, and Jinchao Yue

Investigation on the fracture mechanism of homogenized micro-crack crushing technology for portland cement concrete pavement rehabilitation

Cite as: AIP Advances 9, 075113 (2019); doi: 10.1063/1.5111055
Submitted: 22 May 2019 • Accepted: 8 July 2019 •
Published Online: 19 July 2019

Wenjie Li,[1] Qunlei Zhang,[1] Zihan Zhi,[1] Chun Feng,[2] Yingchun Cai,[1] and Jinchao Yue[1,a)]

AFFILIATIONS

[1]School of Water Conservancy and Environment, Zhengzhou University, Zhengzhou 450001, China
[2]Institute of Mechanics, Chinese Academy of Sciences, Beijing 100190, China

[a)]**Correspondence email:** yuejc@zzu.edu.cn

ABSTRACT

The homogenized micro-crack crushing technology for concrete pavement maintenance has received increased attention in China. To study the fracture mechanism of the homogenized micro-crack crushing technology, a low-velocity impact test system is developed and experiments using concrete slabs of different thicknesses are conducted with different drop heights and hammer weights. Furthermore, the fracture of concrete slabs under impact loading is simulated using the continuous-discontinuous element method. Finally, the fracture mechanism is investigated in a case study. It is concluded that a cylindrical compression–shear fracture surface appears under the impact head while the fractured blocks are still interlocked with each other. The main cracks in the concrete slabs are initiated and propagate parallel to the longer side of the impact head, whereas branch cracks develop perpendicular to the main cracks. These cracks radiate from the center of the impact head. The cracks inside the concrete develop upward from the bottom of the slabs. Because fractured blocks divided by micro-cracks can interlock with themselves and the crack distributions tend to be uniform, it is beneficial for portland cement concrete pavement rehabilitation to be overlaid by a hot-mix asphalt mixture.

I. INTRODUCTION

A. Homogenized micro-crack crushing technology

Portland cement concrete (PCC) pavements are extremely popular because of their simple construction process and strong load-bearing capacity. However, these pavements gradually deteriorate under traffic loading and environmental factors. If the PCC pavement slabs are crushed and excavated for rehabilitation, a large amount of old cement concrete waste will be discarded. This solid waste will occupy landfill sites and may pollute soil and water resources if not handled properly. The recycling of old materials during cement concrete pavement rehabilitation has several environmental and economic benefits. At present, the in-situ utilization of the old concrete pavement involves it being crushed and then overlaid by hot mixed asphalt concrete.[1] Methods of crushing concrete pavements include multiple head breakers, impact compactors, guillotine breakers, resonant pavement breakers, and homogenized micro-crack crushing.[2–5] Using impact compactors and guillotine breakers produces large blocks of cement concrete pavement after crushing. If the hot-mix asphalt concrete is directly overlaid, reflection cracking and cutting-slippage may occur. When cement concrete pavement is crushed by multi-head breakers and resonant pavement breakers, rutting and longitudinal cracking of wheel tracks can easily occur if the hot-mix asphalt concrete is directly overlaid.

In homogenized micro-crack crushing, as shown in Fig. 1, the cement concrete pavement is crushed by special mechanical equipment that produces a low-velocity impact. Before homogenized

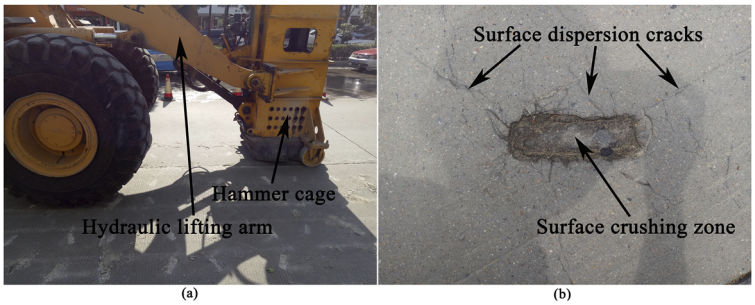

FIG. 1. Homogenized micro-crack crushing. (a) Impact crushing equipment. (b) Impact cracking patterns of pavement.

micro-crack crushing, it is necessary to investigate the pavement conditions and classify them according to the deterioration state. The equipment crushes the concrete pavement slab by slab along the direction of driving. When the pavement deterioration is not serious, the equipment first crushes the pavement along both sides of the slab, and then crushes the center of the slab. When the pavement deterioration is serious, the equipment crushes the concrete pavement slab by slab along the driving direction, and also crushes the movable slabs again. This results in crushed and stable slabs. Some additional debris must be cleaned after homogenized micro-crack crushing. The warpage deformation of the pavement is reduced while the cement concrete pavement is crushed. The bearing capacity of the pavement tends to be uniform, and hot-mix asphalt concrete can be directly overlaid. An impact crushing zone appears in the concrete pavement, and the cracks in the crushing zone diverge. However, there are few studies on the crack propagation mode and the contact mode of fractured blocks in concrete pavement slabs.

B. Overview of studies on fracture mechanism of concrete slabs

Fractures in PCC pavements are one of the main reasons for pavement distress, and also affect the ride quality. Pavement engineers have therefore sought to incorporate an understanding of the fracture mechanics into various pavement evaluation and design procedures.[6] Ramsamooj[7] applied linear elastic fracture mechanics to pavement response models, and later developed stress intensity factors for finite element analysis or layered elastic analysis models.[8] With the introduction of fracture mechanics to pavement design and analysis, finite-element modeling was successfully used to analyze concrete pavements with partial-depth cracks.[9] Ioannides[10] summarized the state of the art in the application of fracture mechanics to pavement engineering, and provided an in-depth discussion of one of the major concerns in such applications, namely the specimen-size effect. A two-step fracture mechanics-based model was developed to predict the occurrence potential of delamination in continuously reinforced concrete pavements.[11] Aure and Ioannides[12] discussed the simulation of crack propagation in concrete beam specimens. The results derived from the beam-as-slab assumption cannot be directly transferred to in-field pavements, which must be considered in terms of both fracture mechanics and the size effect. The fracture of concrete pavement is mainly caused by the development of internal micro-cracks. Aure and Ioannides[13,14] conducted a numerical analysis of the fracture behavior of pavement slabs, and also carried out finite element analysis of crack propagation in pavement slabs-on-grade with aggregate interlocking joints. Fracture mechanics are an important tool in understanding crack formation and propagation in pavement slabs; they also provide models to capture these phenomena. However, research on the fracture mechanism of cement concrete pavement slabs loaded by low-velocity impacts is relatively rare.

In homogenized micro-crack crushing for cement concrete pavements, the crack propagation mode and the contact mode of fractured blocks are key points that should be studied. Low-velocity impact fractures from concrete slab testing will be helpful in understanding the homogenized micro-crack crushing fracture mechanism. Many studies have focused on the impact resistance of these concrete slabs under low-velocity impacts. A number of studies[15–18] referred to the impact testing method of ACI 544.2R-89, which investigates the behavior of concrete slabs containing different fiber types under low-velocity impact. Nia et al.[15] conducted an impact test on plain concrete (PC) and fiber-reinforced concrete (FRC) according to ACI 544, and the results indicated that increasing the fiber volume fraction will increase the impact resistance of the concrete specimens. Steel fibers are more effective at increasing impact resistance than polypropylene fibers. Sakthivel et al.[16] developed a hybrid steel mesh-and-fiber reinforced cementitious composite (HSMFRCC) and studied its impact resistance through low-velocity impact tests. From the experimental results, it was found that the impact resistance of the HSMFRCC test specimens is greater than that of Steel Mesh Reinforced Cementitious Composites (SMRCC). Yahaghi et al.[17] studied the impact resistance behavior of oil palm shell lightweight concretes reinforced by polypropylene (PP) fibers. The results indicated that a simultaneous increase in slab thickness and PP fiber content increases the energy absorption, impact resistance, and crack resistance ratio significantly, but decreases the impact residual strength ratio. Elavarasi and Mohan[18] examined the responses of thin slabs of slurry-infiltrated fibrous concrete (SIFCON) with and without reinforcement under low-velocity impacts. The results show that the incorporation of binary blends of silica fume and slag in the SIFCON matrix produces better performance in terms of strength and durability characteristics. The impact load is often considered in the design of reinforced concrete slabs. A review of studies including impact tests on reinforced concrete slabs indicates that the drop weight impact test is widely used.[19–23] Chen and May[19] investigated the high-mass, low-velocity impact behavior of reinforced concrete slabs, and their investigation enabled a better understanding of the response of reinforced concrete slabs to impact loads. Anil et al.[20] explored the effects of variations in

support conditions on the impact resistance behavior of reinforced concrete slabs. It is observed that the support type and support layouts had a significant effect on the behavior of reinforced concrete slabs subjected to impact loads. Othman and Marzouk[21] developed a three-dimensional finite element (3D-FE) model of RC plates that allows experimental results to be verified. The numerical results confirmed the ability of the calibrated model to predict the response of RC structures under low-velocity loading conditions. Xiao et al.[22,23] studied the effects of loading rates and other parameters on the performances of RC slabs, and proposed a dynamic model to predict the responses of RC slabs under low-velocity impact. From their test results, the load-carrying and energy-absorption capacities of specimens, inertial force, and strain rate were found to increase with higher loading rates, and the results obtained from the 2-D model were further processed to derive the distribution of impact energy during the impact process. Under some extreme loading, the resistance of RC slabs needs to be further improved. There are various methods of improving the resistance of concrete exposed to extreme loading. The enhancement of impact resistance through concrete slab strengthening with both steel fibers and externally bonded FRP sheets was evaluated through low-velocity impact tests. It was noticed that the impact resistance of the steel fiber-reinforced concrete slabs was substantially improved by externally strengthening the fiber-reinforced polymer sheets.[24] Radnic et al.[25] conducted experimental tests on conventional RC slabs and those strengthened with carbon strips under the impact load of a drop hammer. The slabs strengthened with strong carbon fiber strips exhibited somewhat greater ultimate bearing capacity under static and impact loading compared to the conventional RC slabs. High-strength concrete (HSC) is one of the primary cementitious construction materials, and ultra-high-performance fiber-reinforced concrete (UHPFRC) is a relatively new generation of fiber cementitious composites. Their use for the resistance of structural members is increasing, and so their dynamic response has been studied under low-velocity impact. Othman and Marzouk[26,27] investigated the impact resistance of high strength concrete (HSC) and ultra-high-performance fibre-reinforced concrete (UHPFRC) plates under low-velocity impact. The results showed that changes in the reinforcement ratio and/or reinforcement arrangement had no significant effect on the impulse and absorbed energy values for the same impact loading condition, and the UHP-FRC plates exhibited superior damage-control characteristics compared to high-strength concrete (HSC) plates. Most of the aforementioned studies have focused on the impact resistance behavior of fibre-reinforced concrete, reinforced concrete, steel fiber-reinforced concrete, high-strength concrete and ultra-high-performance fibre-reinforced concrete, etc. However, there have been few studies on the micro-crack propagation mode, the contact mode between fractured blocks, and the fracture mechanism of concrete slabs under low-velocity impact.

In order to study the fracture mechanism of homogenized micro-crack crushing of portland cement concrete pavement, a low-velocity impact test system has been developed. Under different impact heights and drop hammer weights, impact fracture tests were conducted using concrete slabs with different thicknesses. The development of micro-cracks, fracture surface morphology, and internal damage of concrete slabs were observed. Furthermore, the dynamic propagation of internal cracks and the fracture surface morphology of the concrete slabs were simulated using a continuous-discontinuous element method (CDEM). Finally, a PCC pavement maintenance project using homogenized micro-crack crushing technology was observed, and the road conditions were surveyed after the laid of hot-mix asphalt concrete overlay.

II. EXPERIMENT

A. Specimens and materials

Ordinary portland cement graded P.O 42.5 was used in the experiments. River sand with a fineness modulus of 2.5 was used as fine aggregate, and gravel with particle sizes of 5–20 mm was used as coarse aggregate. Polycarboxylate superplasticizer was added to obtain a desirable workability. The mix proportions used for the specimens are listed in Table I. BX120-10AA and BX120-50AA strain gauges were employed to measure the strain. Concrete slabs with sizes of 300 mm × 300 mm × 50 mm and 300 mm × 300 mm × 80 mm were prepared for the impact tests. The concrete slabs were demolded after 24 h and cured for 28 days. The compressive strength, axial compression strength, and splitting tensile strength of the concrete material after 28 days were found to be 43.2 MPa, 31 MPa, and 5.1 MPa, respectively.

B. Low-velocity impact test system

The low-velocity impact test system has been developed as a tool for impact experiments. It consists of a drop hammer, auxiliary portal frame, and dynamic data acquisition equipment, as shown in Fig. 2. The drop hammer adheres to the specifications of impact test method ACI 544.2R-89.[28] The drop weight testing sensor gives the impact resistance of fiber concrete for a fixed impact height. The impact resistance was evaluated by the number of blows required to initiate the first crack and the final fracture. Generally, the dynamic response of the fiber concrete cannot be monitored. However, the low-velocity impact test system can perform impact tests for different concrete slab thicknesses loaded by different impact heights and different drop hammer weights. The dynamic response of the impact head and the concrete slab can be monitored synchronously. In the drop hammer impact test device, the portal frame is fixed to a rigid foundation, and the vertical direction of the guide bar is maintained through the top beam. The drop hammer is a hollow cylinder that can fall freely along the guide bar and impact the bearing plate. The impact head, with a rectangular impact area of 20 mm × 54 mm, is located below the bearing plate. The impact heights of the drop hammer impact device can be adjusted freely, and the device is equipped with two different mass hammers (10 kg and 17 kg). The bottom of the hammer body is flat, so the impact load is more uniform when it contacts the surface of the bearing plate during the process of impact testing. Dynamic data acquisition equipment monitors the dynamic

TABLE I. Mix proportion of concrete (kg/m^3).

Water	Cement	Fine agg.	Coarse agg.	Superplasticizer
178	411	718	1078	1.233

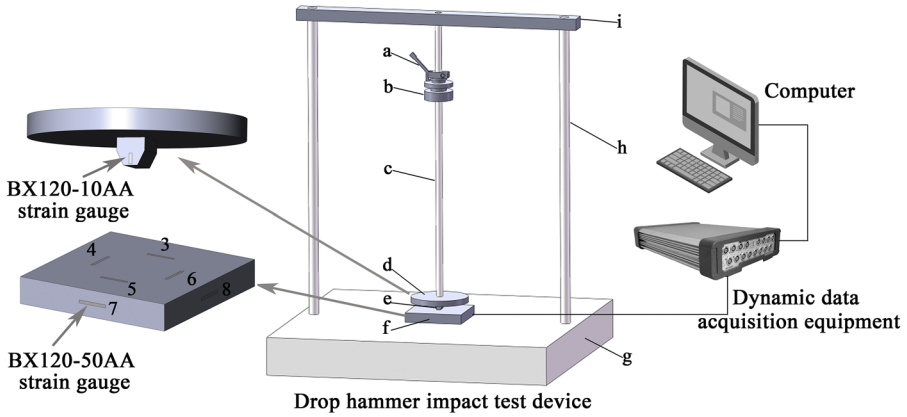

FIG. 2. Low-velocity impact test system. (a) Release mechanism. (b) Drop hammer. (c) Guide bar. (d) Bearing plate. (e) Impact head. (f) Specimen. (g) Rigid foundation. (h) Column. (i) Top beam.

TABLE II. Hammer weights, impact heights, and concrete thicknesses of impact tests.

	50 mm-thick slab				80 mm-thick slab			
Hammer weight (kg)	10	10	10	10	17	17	17	17
Impact height (mm)	600	700	800	900	750	800	850	900

response of the impact head and the concrete slab during impact tests.

C. Experimental process

Considering the different impact heights and drop hammer weights, a series of tests were conducted on the two sizes of concrete slab (see Table II). A number of BX120-50AA strain gauges were arranged on the symmetry axis of the concrete slab, and BX120-10AA strain gauges were placed on the end face of the impact head, as shown in Fig. 2. The strain gauges on top of the concrete slab were numbered 3–6 and those on the sides were numbered 7 and 8. The 3060V dynamic data acquisition module was used to measure the dynamic strain. Moreover, during the low-velocity impact tests, a crack-width observer was employed to observe the development of cracks. In the low-velocity impact tests, when the first visible crack appeared on the top of the slab, the number N_1 of impacts required for initial cracking was recorded. As while as the initial cracking, when the main crack ran through the concrete slab from its bottom to its surface, the number N_2 of impacts required for final fracture was recorded.

III. RESULTS AND DISCUSSION

A. Impact test of 50 mm-thick concrete slab

First, the 300 mm × 300 mm × 50 mm (length × width × thickness) concrete slab was tested. N_1 and N_2 at impact heights of 600 mm, 700 mm, 800 mm, and 900 mm are presented in Table III. The strain on the impact head under the four different impact heights is shown in Fig. 3. With the increase of impact height, the impact number gradually decreased. After cracks appeared on the top of the concrete slab, subsequent impacts caused the cracks to expand rapidly, and then the slab failed. The total impact time was about 7.8 ms. The maximum strain values of the impact head from different drop heights were -294.49 με, -319.84 με, -339.20 με, and -356.92 με, respectively.

In order to study the relationship between strain and crack propagation, the impact height of 600 mm was taken as an example (see Fig. 4). When the impact head strain reached the peak of -294.49 με, the strain at points 3 and 5 reached peaks of -327.68 με and -372.68 με at the same time. However, points 4 and 6 did not reach their peak strain values of -365.72 με and -93.94 με until 1.56 ms

TABLE III. Impact number for the 50 mm-thick concrete slab under different impact heights.

Drop weight (kg)	Drop height (mm)	Impact number of first crack	Impact number of final fracture
10	600	4	7
10	700	3	5
10	800	2	3
10	900	1	2

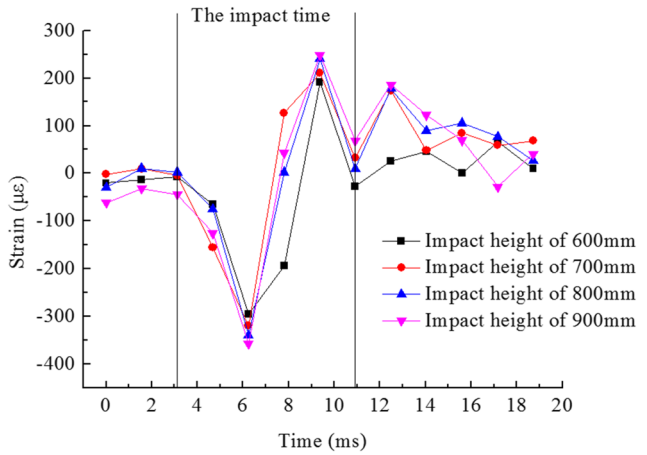

FIG. 3. Strain of the impact head under different impact heights of 50mm-thick slabs.

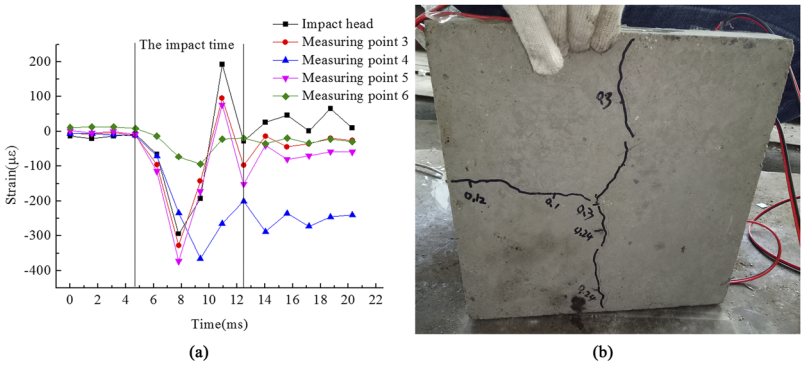

FIG. 4. Relationship between strain and crack propagation. (a) The strain under the impact height of 600mm. (b) Bottom of 50mm-thick concrete slab.

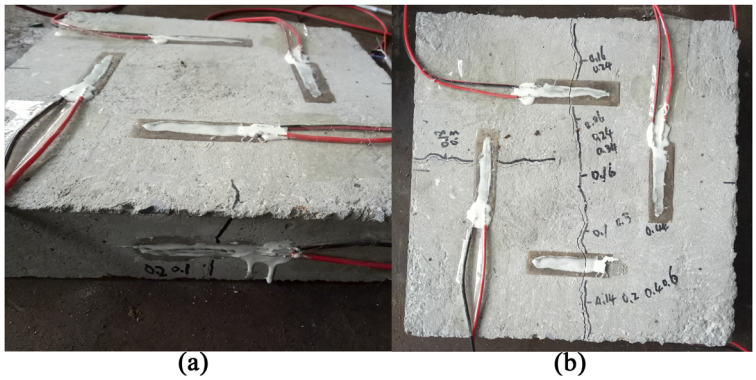

FIG. 5. Crack propagation in the 50 mm-thick concrete slab. (a) Side and top cracks. (b) Failed concrete slab.

later. After the first impact, a main crack propagated along the longitudinal direction of the impact head and a branch crack propagated along the transverse direction at the bottom of the concrete slab. According to the strain of the concrete slab, the development of the main crack was earlier than that of the branch crack.

The crack propagation in the 50 mm-thick concrete slab under low-velocity impact is shown in Fig. 5. Under low-velocity impact, the bottom of the concrete slab cracked first, and then cracks developed from the bottom to the side of the slab, before finally extending to the top of the concrete slab. After repeated impacts, the main crack appeared along the longitudinal direction of the impact head, and the branch crack appeared along the transverse direction. Once the main crack ran through the concrete slab, the slab failed. When the slab failed, the average widths of the main crack and branch crack were 0.41 mm and 0.30 mm, respectively.

In order to observe the fracture surface morphology of concrete slabs and the crack propagation and damage inside the slabs, one failed concrete slab was cut along the main crack, and another slab was cut twice along the transverse direction of the impact head, as shown in Fig. 6. The main fracture surface was not smooth, and

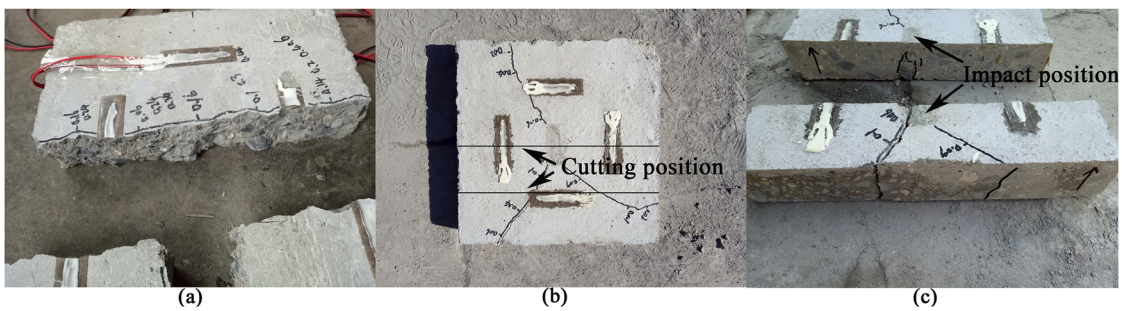

FIG. 6. Main fracture surface and cutting surfaces. (a) Main fracture surface. (b) Cutting position. (c) Cutting surfaces.

TABLE IV. Impact number for the 80 mm-thick concrete slab under different impact heights.

Drop weight (kg)	Drop height (mm)	Impact number of first crack	Impact number of final fracture
17	750	6	8
17	800	5	7
17	850	2	4
17	900	1	3

the fracture mainly ran along the interface between aggregate and mortar. Almost no aggregate breakage was observed. A punching fracture occurred in the concrete slab under the impact head, and there were many vertical cracks running upward from the bottom. Far from the impact center, the inclination of the main crack was smaller, while that of the branch crack was larger.

B. Impact test of 80 mm-thick concrete slab

The 300 mm × 300 mm × 80 mm concrete slab was tested, and N_1 and N_2 were recorded for impact heights of 750 mm, 800 mm, 850 mm, and 900 mm. The results are presented in Table IV. Similar to the 50 mm-thick concrete slab, an increase in impact height resulted in a gradual decrease in the impact number of the first crack and the final fracture. However, for the same impact height, N_1 and N_2 were larger than that for the 50 mm-thick slab.

The crack propagation is illustrated in Fig. 7. Similar to the 50 mm-thick concrete slab, cracks first appeared in the bottom of the 80 mm-thick concrete slab and then propagated to the side after multiple impacts. Finally, the main crack and the branch crack were formed, and the slab failed. When the slab failed, the average widths of the main crack and the branch crack were 0.82 mm and 0.16 mm, respectively.

In order to observe the fracture surface morphology and internal damage of the 80 mm-thick concrete slab, the concrete slabs were cut along the main crack and along the transverse direction of the impact head, as shown in Fig. 8. The main fracture surface of the concrete slab was convex and concave, and the roughness of the convex–concave sections was larger than that of the 50 mm-thick concrete slab. The fractured blocks were interlocked with each other. The fracture mainly occurred along the interface between aggregate and mortar, and some aggregates were broken. The concrete slab under the impact head was punched, and two vertical cracks under the impact center formed a columnar fracture zone. In this columnar fracture zone, micro-cracks had developed along the interface between the aggregates and cement mortar, and the local concrete was crushed near the bottom of the slab. At the bottom of the slab, the main crack propagated from the impact center to the slab edge. The branch crack first propagated from the impact center to the slab edge, and then formed multiple branch cracks near the edge of the slab.

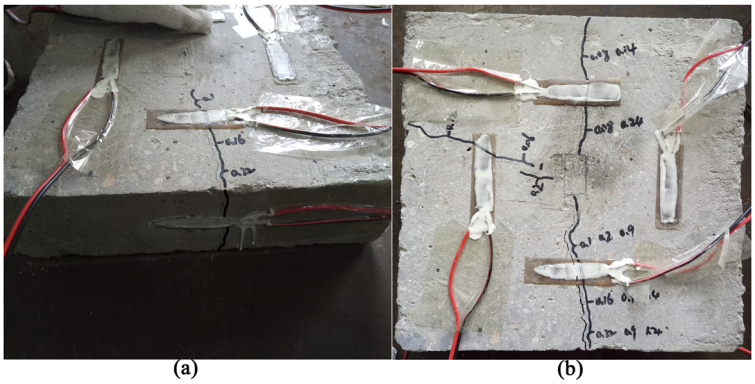

(a) (b)

FIG. 7. Crack propagation in 80mm-thick concrete slab. (a) Side and top cracks. (b) Failed concrete slab.

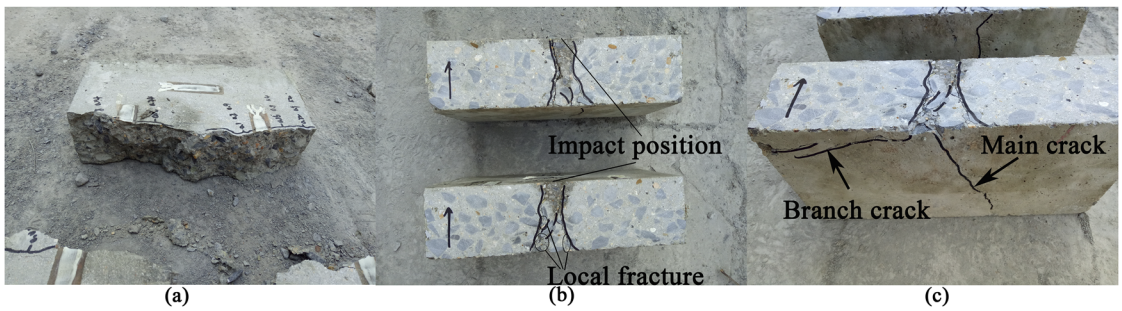

(a) (b) (c)

FIG. 8. Main fracture surface and cutting surface. (a) Main fracture surface. (b) Cutting surface. (c) The bottom cracks.

C. Summary

The bottom of the concrete slab cracked first under low-velocity impact. The main crack developed earlier than the branch crack. After repeated impacts, the slab failed once the main crack ran through the concrete slab. Moreover, for the same impact height, the numbers of impacts required for the first crack and the final fracture of the 80 mm-thick concrete slab were greater than that for the 50 mm-thick slab. The average widths of the main crack and the branch crack in both kinds of concrete slabs were ultimately both less than 1 mm. Comparing the fracture surface morphology and internal crack development of the 50 mm-thick concrete slab and the 80 mm-thick concrete slab, it can be seen that under low-velocity impact, the roughness of the convexity–concavity of the fracture surface increases with the slab thickness. The 80 mm-thick concrete slab has a larger compression–shear failure zone and larger crack inclination angle, and the interlocked effect of the fractured block is better than that of the 50 mm-thick concrete slab.

IV. NUMERICAL SIMULATIONS

A. Method

In order to observe the development and shape of the internal fracture surface of concrete slabs during impact tests, numerical simulations were performed to supplement the experiments. The numerical simulations used the continuous-discontinuous element method (CDEM), which couples finite element calculations with discrete element calculations. This technique allows finite element calculations to be conducted inside block elements and discrete element calculations at the boundaries of block elements. Through the fracture of interface elements, this method simulates the deformation and motion characteristics of a material in a continuous state, and also realizes the failure process of a material from the continuous state to the discontinuous state. Ma et al.[29] investigated the propagation of micro-cracks under excavation-induced unloading conditions during the construction of underground storage caverns, and Ju et al.[30] studied the processes of crack initiation and propagation in a heterogeneous material based on the continuous-discontinuous element method (CDEM). The governing equations of continuous-discontinuous element method (CDEM) were derived by Jing and Stephansson,[31] and include dynamic equilibrium equations, linear elastic constitutive equations, and displacement–strain relations. Details of the computational model and cracking criterion for continuous-discontinuous element method (CDEM) can be found in previous reports.[29,30]

TABLE V. Material model properties of hammer, bearing plate, impact head, and concrete slab.

	Hammer, bearing plate, and impact head	Concrete slab
Density	7850 kg/m^3	2400 kg/m^3
Young's modulus	200 GPa	28 GPa
Poisson's ratio	0.25	0.2
Uniaxial compressive strength	-	40 MPa
Tensile strength	-	5 MPa

B. Numerical modeling

When the different impact heights applied to the two kinds of concrete slabs are converted into impact velocities, they range from 3–5 m/s. In order to observe the dynamic propagation of internal cracks and the fracture surface morphology of concrete slabs, numerical simulations were conducted. In low-velocity impact tests, the first impact is very important for the cracking of concrete slabs. Therefore, impact velocities of 3 m/s, 4 m/s, 5 m/s, and 6 m/s were selected to study the dynamic cracking process of concrete slabs under the first impact. Models of the drop hammer, bearing plate, impact head, and concrete slab were created separately, and the appropriate contact conditions were set between each model component. The drop hammers were modeled as cylinders with the same mass as the hammers. The numerical models are shown in Fig. 9. The drop hammer, load bearing plate, and impact head were analyzed using the continuous element method, whereas the impact fracture of the concrete slabs was evaluated using discrete element theory. The drop hammer was meshed with hexahedral elements, whereas the bearing plate and impact head were meshed with tetrahedral elements. To realize the random development of cracks, the concrete slabs were meshed with tetrahedral elements. The 50 mm-thick concrete slab was meshed with 35105 tetrahedral elements with dimensions of 10 mm. The 80 mm-thick slab was meshed with 55018 tetrahedral elements with dimensions of 10 mm. The material properties of the drop hammer, bearing plate, impact head, and concrete slab are listed in Table V.

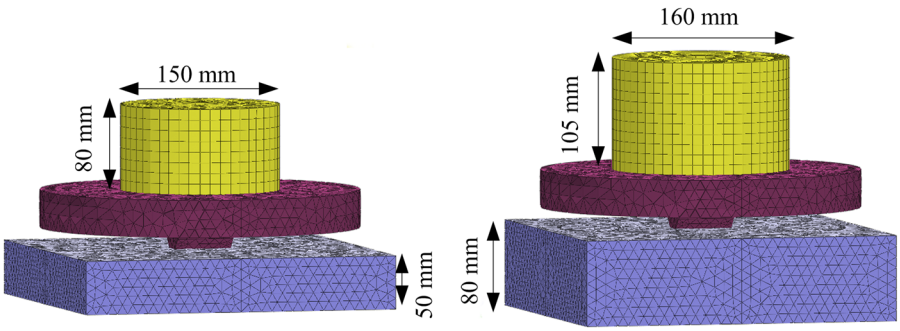

FIG. 9. Numerical models of the impact tests.

C. Crack propagation patterns

The development of cracks in the 50 mm-thick and 80 mm-thick slabs under impact velocities of 3 m/s, 4 m/s, 5 m/s, and 6 m/s is displayed in Figs. 10 and 11. At lower impact velocities, compression–shear cracks appear first on the top of the concrete slabs. As the impact velocity increases, tensile cracks appear along the longitudinal direction of the impact head in the center of the slab bottom. As the impact velocity increases further, the cracks run through the concrete slab along the longitudinal direction of the impact head, and then the concrete slab fails. When the impact velocity was 4 m/s, compression–shear cracks appeared on the top of the 50 mm-thick slab and tension cracks appeared on the bottom. However, similar cracks only occurred in the 80 mm-thick slab when the impact velocity was 5 m/s. When the impact velocity was 6 m/s, the main crack ran right through the 50 mm-thick slab, whereas it did not quite pass through the 80 mm-thick slab. However, once cracks occurred on both the top and bottom of the concrete slabs, the crack propagation patterns were similar. As shown in Figs. 5–8, the concrete slabs cracked under low-velocity impact, with the main crack developing along the longitudinal direction of the impact head and some compression–shear cracks appearing in the concrete slab at the impact center position. The numerical simulation results are in good agreement with the experimental results.

D. Analysis of internal fractures

The dynamic fracture process of the 50 mm-thick and 80 mm-thick slabs under an impact velocity of 6 m/s is shown in Figs. 12 and 13. Under low-velocity impact, compression–shear cracks first appeared at the top of the two kinds of concrete slabs, and the fracture gradually developed from top to bottom to form a cylindrical fracture surface. At the same time, tensile cracks appeared at the center of the bottom surface. Along the longitudinal direction of the impact head, the fracture surface extended from the center to the edge of the slab until it ran through the concrete slab, and then the concrete slab failed. Compared with the 50 mm-thick slab, the 80 mm-thick slab exhibited a more regular cylindrical fracture surface and a deeper degree of convexity and concavity from the main fracture surface. From Figs. 6 and 8, we conclude the fracture surface and crack morphology are basically in agreement with the experimental results.

E. Discussion

Under low-velocity impact, the propagation mode of cracks in concrete slabs determines the shape of the fracture surface, and directly affects the interlocking effect of the fractured blocks. These numerical simulations supplement the shortcomings of the tests, allowing the dynamic development process of the internal fracture

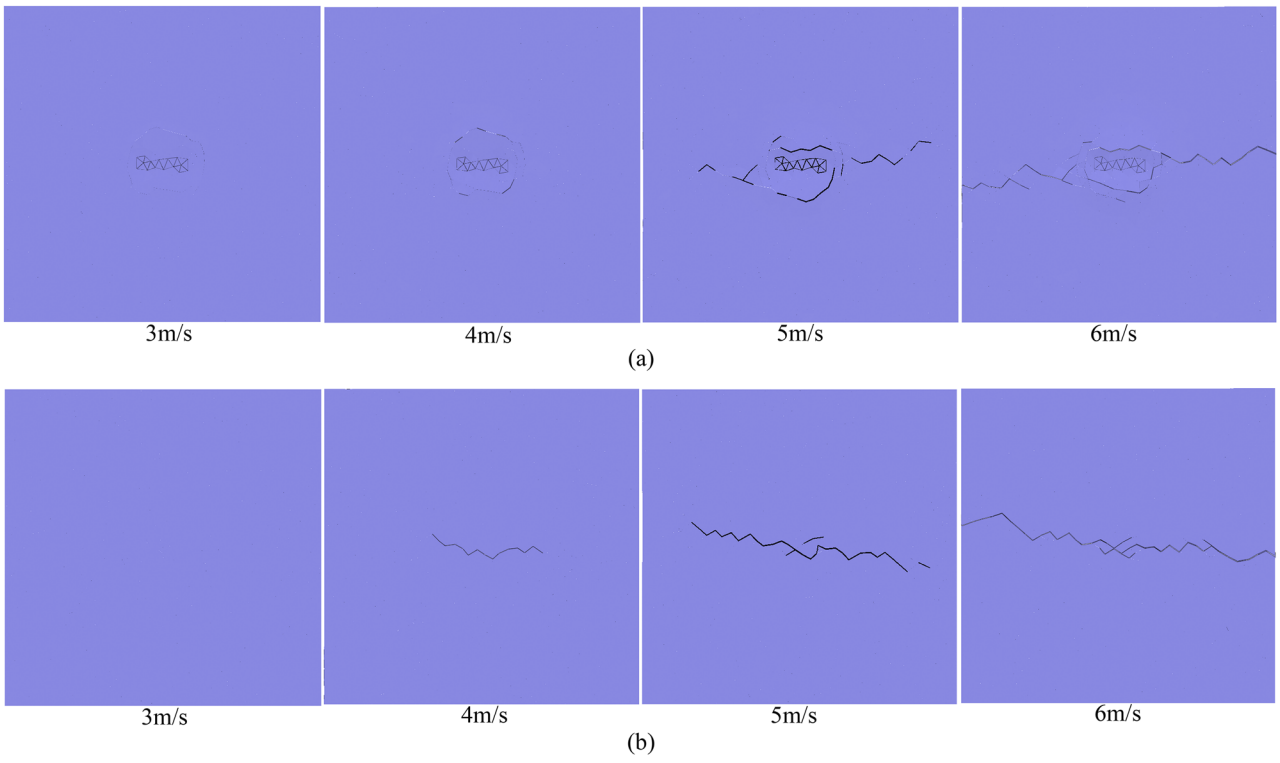

FIG. 10. Development of cracks in the 50mm-thick concrete slab. (a) Top surfaces. (b) Bottom surfaces.

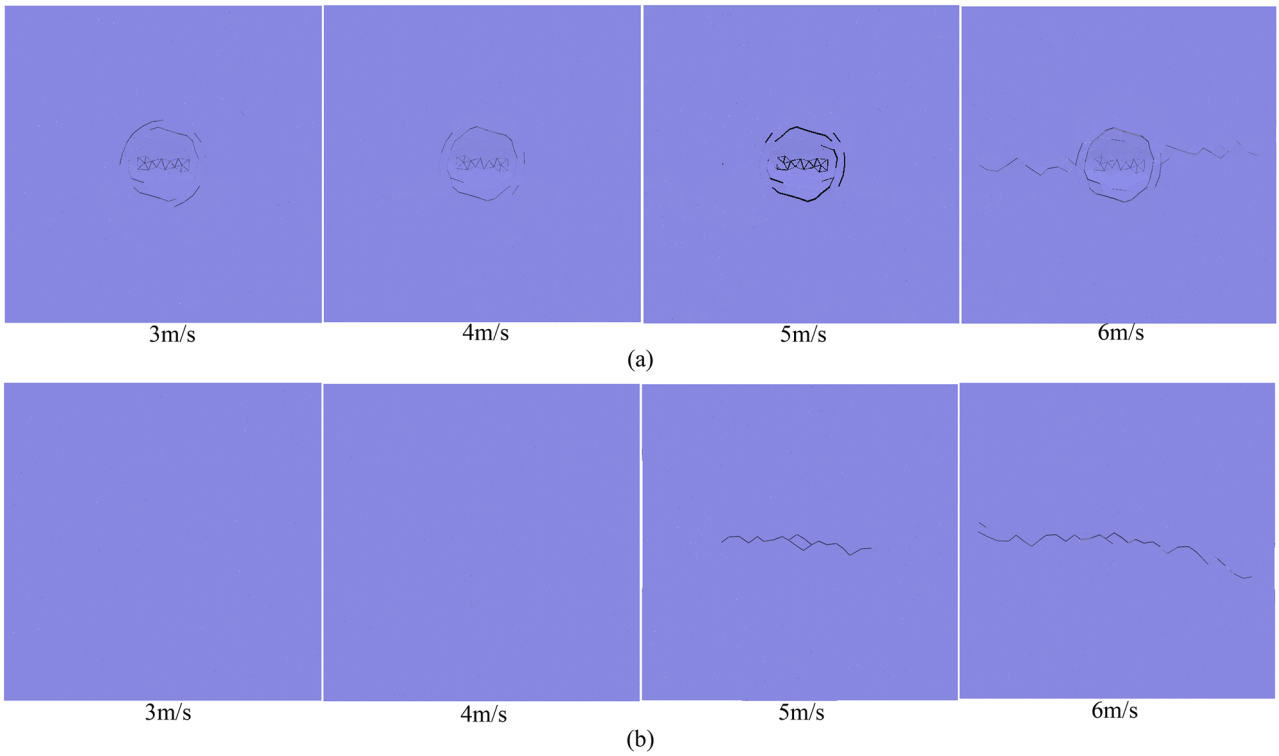

FIG. 11. Development of cracks in the 80mm-thick concrete slab. (a) Top surfaces. (b) Bottom surfaces.

of concrete slabs to be analyzed. As shown in Figs. 12 and 13, under low-velocity impact, the concrete slabs first cracked in the contact area of the impact head. The cracks gradually extended to the interior of the concrete slab to form a cylindrical compression–shear failure zone. At the same time, cracks appeared in the center of the bottom of the concrete slabs. The crack surface gradually extended from the middle of the slabs to the edge, and eventually ran through the slabs.

The experimental and numerical results show that the main crack in concrete slabs propagates along the longitudinal

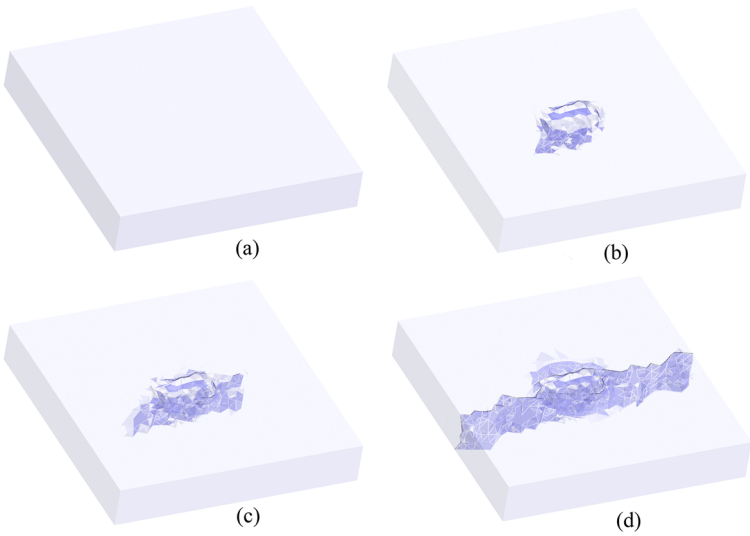

FIG. 12. Dynamic cracking process of 50mm-thick concrete slab. (a) Calculation steps 1000. (b) Calculation steps 23000. (c) Calculation steps 40000. (d) Calculation steps 80000.

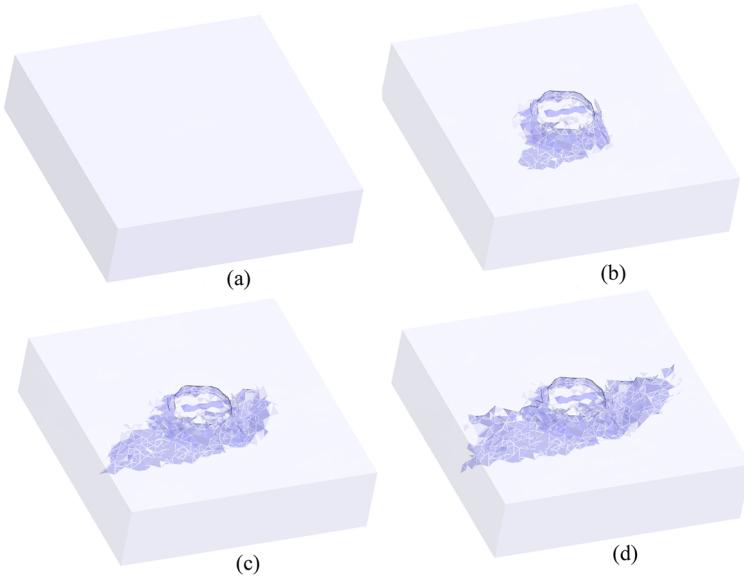

FIG. 13. Dynamic cracking process of 80mm-thick concrete slab. (a) Calculation steps 1000. (b) Calculation steps 52000. (c) Calculation steps 80000. (d) Calculation steps 100000.

direction of the impact head, whereas branch cracks develop along the transverse direction. Moreover, the impact area on top of the concrete slabs cracks first, and then an annular compression–shear failure zone appears in the interior of the slabs. Furthermore, the internal fracture surface extends along the longitudinal direction of the impact head until it runs through the concrete slab. The fracture surface of the concrete slab is uneven, and the fractured blocks are still interlocked with each other.

V. PRACTICAL APPLICATION

The fracture mechanism of concrete slabs has been studied experimentally and by numerical simulations. The propagation mode of the main crack and branch cracks and the fracture surface morphology in the slab were obtained. However, many factors affect the crushing of concrete pavement slabs in actual pavement rehabilitation, so it is necessary to verify the fracture mechanism of concrete pavement slabs in a real-world scenario.

A. Project background

The G106 National Road Zhumadian from Xinyang junction to Baoxin Town was originally designed as a second-class highway. This section measures 12.779 km, running from K920+882 to K933+661, and the cement concrete pavement and the subgrade are 12 m and 15 m wide, respectively. The thickness of the jointed plain concrete pavement is 260 mm, and that of the cement stabilized crashed stone base is 180 mm. The volume of traffic flow and heavy vehicles led to serious pavement distress, particularly transverse cracking, longitudinal cracking, block cracking, and corner breaks, as shown in Fig. 14. To restore the pavement performance, homogenized micro-crack crushing was used to crush the concrete pavement, and then hot-mix asphalt concrete was overlaid, with a 40 mm AC-16 lower layer and 40 mm AC-13 upper layer.

B. Homogenized micro-crack crushing treatment

The cement concrete pavement was crushed by homogenized micro-crack crushing equipment. The mass of the drop hammer

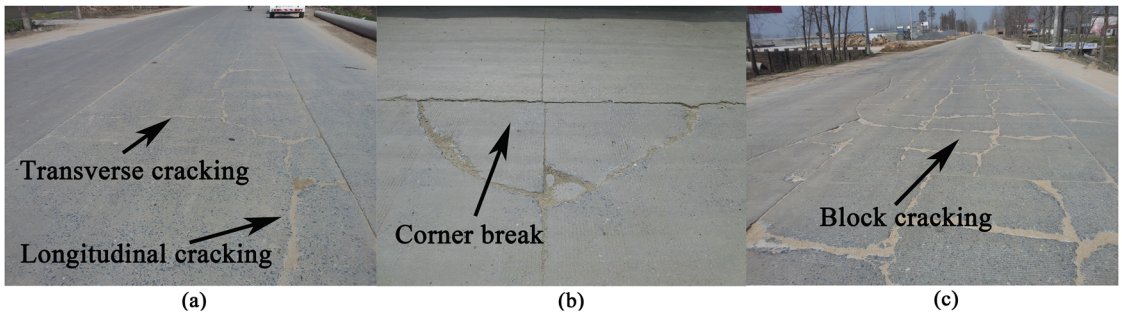

FIG. 14. Pavement distress. (a) Transverse and longitudinal cracking. (b) Corner break. (c) Blocking cracking.

FIG. 15. Cement concrete pavement before and after crushing. (a) Pavement before crushing. (b) Pavement after crushing. (c) After debris cleaning.

was 3000 kg, and the impact height is divided into four grades of 0.8 m, 1.2 m, 1.7 m, and 2.2 m. Following a pavement condition survey, the impact height of 1.2 m was selected. The equipment first crushes the pavement along both sides of the slab, and then along the center. The cement concrete pavement before and after crushing is shown in Fig. 15. After the concrete pavement had been crushed, there was some debris on the surface of the pavement. Once the debris had been cleaned, micro-cracks appeared on the

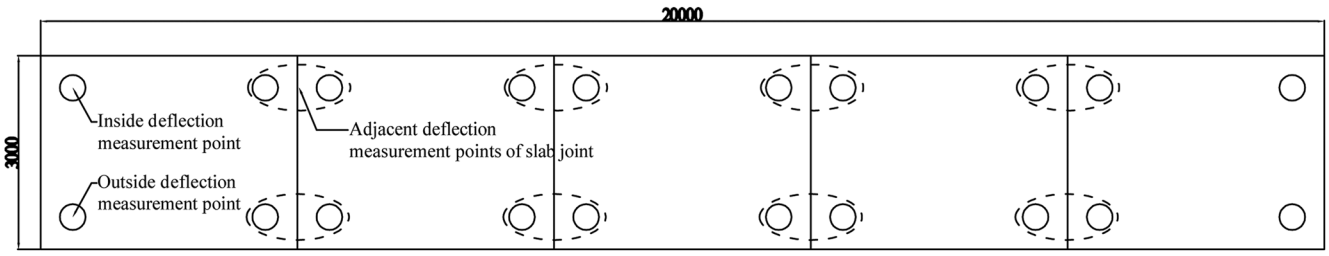

FIG. 16. Location of the deflection measurements.

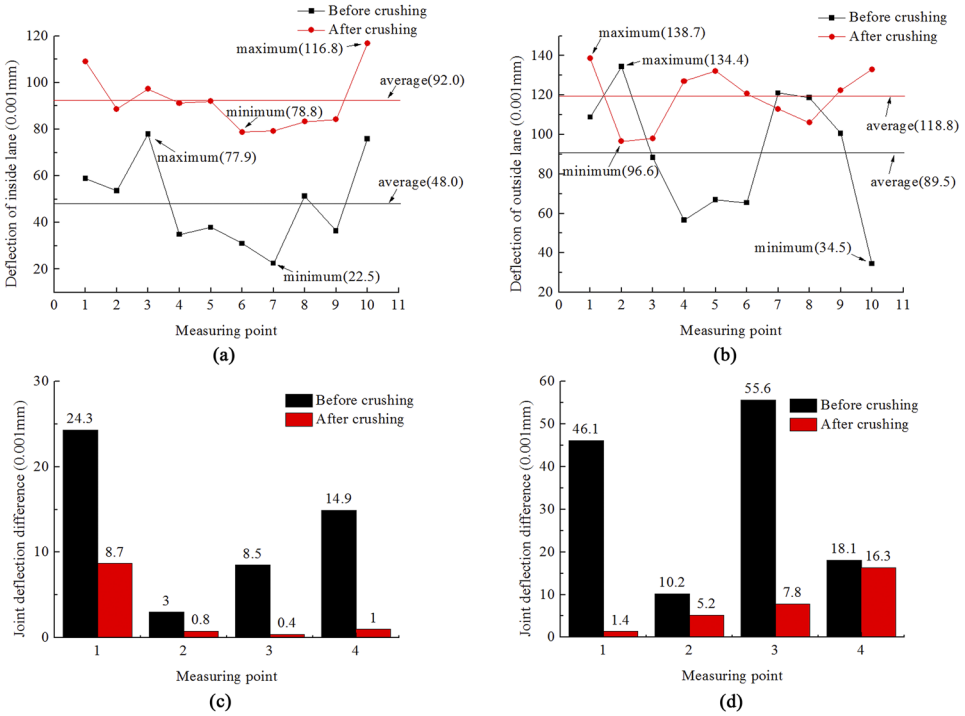

FIG. 17. Deflection and joint deflection difference before and after crushing. (a) Deflection of inside lane. (b) Deflection of outside lane. (c) Joint deflection difference of inside lane. (d) Joint deflection difference of outside lane.

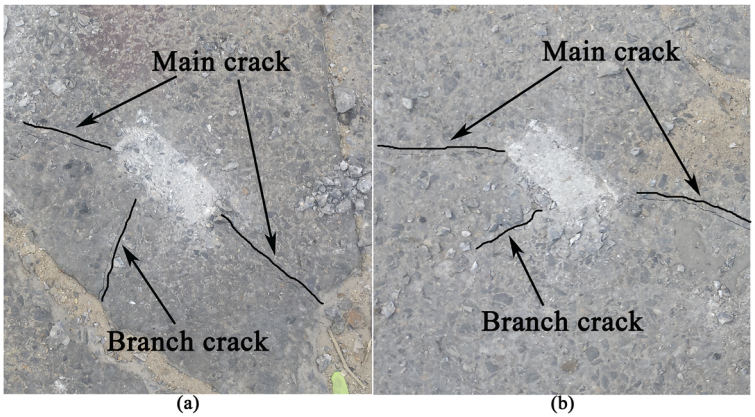

FIG. 18. Development of main crack and branch crack after crushing. (a) Surface crushed zone I. (b) Surface crushed zone II.

pavement, and the fractured blocks were nearly uniformly distributed in space.

The deflection of a 20-m overtaking lane was measured before and after crushing. The locations of the deflection measurements are shown in Fig. 16. The deflection values from the inside and outside of the overtaking lane are shown in Fig. 17.

The difference between the average deflection on the inside and the outside of the overtaking lane was 41.5 (0.001 mm) before homogenized micro-crack crushing. This had decreased to 26.8 (0.001mm) after crushing, as shown in Figs. 17(a) and 17(b). The deflection values of the inside and outside of the overtaking lane were more discrete, with coefficients of variation of 37% and 35%, respectively, before homogenized micro-crack crushing. The dispersion degree of the deflection values of the inside and outside became smaller after crushing, having coefficients of variation of 13% and 12%, respectively. Generally, the coefficients of variation of the overtaking lane deflection values reduced by about 23% after homogenized micro-crack crushing. The maximum joint deflection differences of the inside and outside of the overtaking lane were 24.3 (0.001 mm) and 55.6 (0.001 mm) before homogenized micro-crack crushing, as shown in Figs. 17(c) and 17(d). After crushing, these values were 8.7 (0.001 mm) and 7.8 (0.001 mm), respectively. The joint deflection differences decreased significantly after homogenized micro-crack crushing. The crushing process increased the average value of the pavement deflection, but greatly reduced the dispersion degree of the pavement deflection value, and improved the uniformity. The joint deflection difference was decreased by the interlocking between fractured blocks.

C. Verification of crack development

After homogenized micro-crack crushing, a uniform distribution of cracks appeared on the concrete pavement, and the surface crushed zone could be observed, as shown in Fig. 18. The main crack developed along the longitudinal direction of the impact head and the branch cracks developed along the transverse direction. When the lateral side of the impact head was closer to the slab edge, the branch cracks developed to the slab edge, and when the lateral side of the impact head was far from the slab edge, the development of the branch cracks was limited. However, the development of the main cracks was less affected by the slab size.

To observe internal cracks in the pavement, some cores were extracted (see Fig. 19). The bottom of the concrete slab cracked first

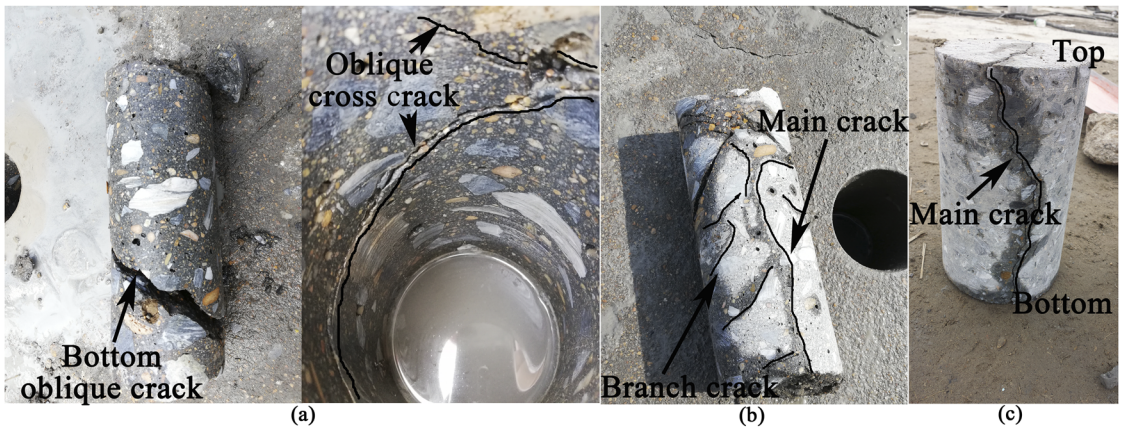

FIG. 19. Core samples after homogenized micro-crack crushing. (a) Core I and core hole. (b) Core II. (c) Core III.

FIG. 20. Pavement conditions after the laying of hot-mix asphalt concrete overlay. (a) After one month. (b) After six months. (c) After one year. (d) Almost two years.

after the pavement slab was crushed, as shown in Fig. 19(a). The cracks developed upward, and there were many oblique cracks crossing. Figure 19(b) shows a main crack running through the concrete slab, and several branch cracks progressing from the bottom to the top in oblique intersection with the main crack. Figure 19(c) shows that the main crack ran through the concrete slab and developed along the direction of inclination while the fractured blocks were still closely interlocked.

The development of the main crack and branch crack on the pavement surface, the development of cracks inside the pavement slab, and the contact mode of fractured blocks are consistent with the experimental and numerical simulation results. Under low-velocity impact, the crack development of the concrete slab and the contact mode of fractured blocks have been verified in situ.

D. Overlay

The hot-mix asphalt concrete was directly overlaid after homogenized micro-crack crushing, with a 40 mm AC-16 lower layer and 40 mm AC-13 upper layer. Figure 20 shows the pavement conditions after one month, six months, one year, and almost two years. After almost two years, the International Roughness Index (IRI), deflection, and texture depth of the hot-mix asphalt concrete overlay were tested in accordance with the requirements of the Inspection and Evaluation Quality Standards for Highway Engineering.[32] The results are presented in Table VI. After almost two years of service, the pavement exhibits no obvious distress and its condition is good.

TABLE VI. Results of IRI, deflection, and texture depth.

	IRI (m/km)	Deflection (0.001 mm)	Texture depth (mm)
Mean	2.1	65.2	0.3
Standard deviation	0.9	12.8	0.1
Variation coefficient	0.4	0.2	0.3

VI. CONCLUSIONS

This paper has described a low-velocity impact test system. The fracture mechanism of homogenized micro-crack crushing technology has been investigated through experiments, numerical simulations, and field tests. The following conclusions can be drawn.

Under low-velocity impact, the main crack in concrete slab develops along the longitudinal direction of the impact head, whereas the branch cracks develop along the transverse direction. The main crack develops earlier than the branch crack. When the concrete slab fails, the average width of the main crack is slightly larger than that of the branch cracks, but both are less than 1 mm wide. The internal cracks develop upward from the bottom, the main cracks and branch cracks intersect obliquely.

Compression–shear cracks first appear in the impact center of the top surface of the concrete slab, and then a columnar shear failure surface appears in the concrete slab. Gradually, the main tensile crack appears in the center of the bottom of the concrete slab and develops along the longitudinal direction of the impact head. The fracture surface of the concrete slab is uneven. The fractured blocks of concrete slab remain interlocked with each other after crushing; thicker slabs have a better interlocking effect.

The deflection of concrete pavement becomes more uniform after homogenized micro-crack crushing. The crushing technology provides good conditions for constructing the overlay in concrete pavement rehabilitation.

ACKNOWLEDGMENTS

This research was funded by the National Key Research and Development Program of China (Grant No. 2018YFC1505504) and Henan Provincial Department of Transportation (Project no. 2018J4).

REFERENCES

[1] J. Ma, S. Z. Sun, H. T. Rui *et al.*, "Review on China's road construction machinery research progress: 2018," China Journal of Highway and Transport **31**(6), 136–139 (2018) (in Chinese).
[2] H. Ceylan, K. Gopalakrishnan, B. J. Coree, T. Kota, and R. Mathews, "Rehabilitation of concrete pavements utilizing rubblization: A mechanistic based approach to HMA overlay thickness design," International Journal of Pavement Engineering **9**(1), 45–57 (2008).
[3] D. H. Chen, Q. L. Huang, and J. M. Ling, "Shanghai's experience on utilizing the rubblization for jointed concrete pavement rehabilitation," Journal of Performance of Constructed Facilities **22**(6), 398–407 (2008).
[4] X. Qiu, J. M. Ling, and F. Wang, "Concrete pavement rehabilitation procedure using resonant rubblization technology and mechanical-empirical based overlay design," Canadian Journal of Civil Engineering **41**(1), 32–39 (2014).
[5] Z. S. Ge, H. Li, Z. T. Han, and Q. S. Zhang, "Properties of cold mix asphalt mixtures with reclaimed granular aggregate from crushed PCC pavement," Construction and Building Materials **77**, 404–408 (2015).
[6] D. Tompkins, L. Khazanovich, and J. E. Bolander, "Lattice modelling of fracture in composite concrete pavements and overlays," International Journal of Pavement Engineering **16**(1), 56–68 (2015).
[7] D. V. Ramsamooj, "Fracture of highway and airport pavements," Engineering Fracture Mechanics **44**(4), 609–626 (1993).
[8] D. V. Ramsamooj, G. S. Lin, and J. Ramadan, "Stresses at joints and cracks in highway and airport pavements," Engineering Fracture Mechanics **60**(5), 507–518 (1998).
[9] J. R. Roesler and L. Khazanovich, "Finite-element analysis of portland cement concrete pavements with cracks," Transportation Research Record **1568**, 1–9 (1997).
[10] A. M. Ioannides, "Fracture mechanics in pavement engineering: The specimen size effect," Transportation Research Record **1568**, 10–16 (1997).
[11] J. Y. Liu, X. Zhang, and D. G. Zollinger, "Two-step fracture mechanics-based approach to assess early-age delamination distress," Transportation Research Record **2016**, 76–84 (2007).
[12] A. M. Ioannides and T. W. Aure, "Simulation of crack propagation in concrete beams with cohesive elements in ABAQUS," Transportation Research Record **2154**, 12–21 (2010).
[13] T. W. Aure and A. M. Ioannides, "Numerical analysis of fracture process in pavement slabs," Canadian Journal of Civil Engineering **39**(5), 506–514 (2012).
[14] T. W. Aure and A. M. Ioannides, "Fracture analysis of aggregate interlock jointed slabs-on-grade," Construction and Building Materials **77**, 340–348 (2015).
[15] A. A. Nia, M. Hedayatian, M. Nili, and V. A. Sabet, "An experimental and numerical study on how steel and polypropylene fibers affect the impact resistance in fiber-reinforced concrete," International Journal of Impact Engineering **46**, 62–73 (2012).
[16] P. B. Sakthivel, A. Ravichandran, and N. Alagamurthi, "Impact strength of hybrid steel mesh-and-fiber reinforced cementitious composites," KSCE Journal of Civil Engineering **19**(5), 1385–1395 (2015).
[17] J. Yahaghi, Z. C. Muda, and S. B. Beddu, "Impact resistance of oil palm shells concrete reinforced with polypropylene fibre," Construction and Building Materials **123**, 394–403 (2016).
[18] D. Elavarasi and K. S. R. Mohan, "On low-velocity impact response of SIFCON slabs under drop hammer impact loading," Construction and Building Materials **160**, 127–135 (2018).
[19] Y. Chen and I. M. May, "Reinforced concrete members under drop-weight impacts," Proceedings of the Institution of Civil Engineers-Structures and Buildings **162**(1), 45–56 (2009).
[20] O. Anil, E. Kantar, and M. C. Yilmaz, "Low velocity impact behavior of RC slabs with different support types," Construction and Building Materials **93**, 1078–1088 (2015).
[21] H. Othman and H. Marzouk, "Finite-element analysis of reinforced concrete plates subjected to repeated impact loads," Journal of Structural Engineering **143**(9), 04017120 (2017).
[22] Y. Xiao, B. Li, and K. Fujikake, "Experimental study of reinforced concrete slabs under different loading rates," ACI Structural Journal **113**(1), 157–168 (2016).
[23] Y. Xiao, B. Li, and K. Fujikake, "Predicting response of reinforced concrete slabs under low-velocity impact," Magazine of Concrete Research **69**(19), 996–1010 (2017).
[24] D. Y. Yoo and Y. S. Yoon, "Influence of steel fibers and fiber-reinforced polymers on the impact resistance of one-way concrete slabs," Journal of Composite Materials **48**(6), 695–706 (2014).
[25] J. Radnic, D. Matesan, N. Grgic, and G. Baloevic, "Impact testing of RC slabs strengthened with CFRP strips," Composite Structures **121**, 90–103 (2015).
[26] H. Othman and H. Marzouk, "An experimental investigation on the effect of steel reinforcement on impact response of reinforced concrete plates," International Journal of Impact Engineering **88**, 12–21 (2016).
[27] H. Othman and H. Marzouk, "Impact response of ultra-high-performance reinforced concrete plates," ACI Structural Journal **113**(6), 1325–1334 (2016).
[28] ACI Committee 544, ACI 544.2R-89, Measurement of properties of fiber reinforced concrete, Detroit, American Concrete Institute, 1999.
[29] K. Ma, C. A. Tang, L. X. Wang, D. H. Tang, D. Y. Zhuang, Q. B. Zhang, and J. Zhao, "Stability analysis of underground oil storage caverns by an integrated numerical and microseismic monitoring approach," Tunnelling and Underground Space Technology **54**, 81–91 (2016).
[30] Y. Ju, P. Liu, J. L. Chen, Y. M. Yang, and P. G. Ranjith, "CDEM-based analysis of the 3D initiation and propagation of hydrofracturing cracks in heterogeneous glutenites," Journal of Natural Gas Science and Engineering **35**, 614–623 (2016).
[31] L. R. Jing and O. Stephansson, *Fundamentals of Discrete Element Methods for Rock Engineering: Theory and Applications* (Elsevier, 2007).
[32] Research Institute of Highway Ministry of Transport, JTG F80/1-2017 Inspection and Evaluation Quality Standards for Highway Engineering Section 1 Civil Engineering, Beijing, China Communication Press, 2017.